Hybrid Composites of Monodisperse π-Conjugated Rodlike Organic Compounds and Semiconductor Quantum Particles

Volker Hensel,[a] Adelheid Godt,[b] Ronit Popovitz-Biro,[a] Hagai Cohen,[a] Torben R. Jensen,[c] Kristian Kjaer,[c] Isabelle Weissbuch,[a] Efrat Lifshitz,[d] and Meir Lahav*[a]

Abstract: Composite materials of quantum particles (Q-particles) arranged in layers within crystalline powders of π-conjugated, rodlike dicarboxylic acids are reported. The synthesis of the composites, either as three-dimensional crystals or as thin films at the air–water interface, comprises a two-step process: 1) The preparation of the Cd salts **6(Cd)**, **8(Cd)** or Pb salts **6(Pb)**, **8(Pb)** of the oligo(*p*-phenyleneethynylene)dicarboxylic acids **6(H)**, **8(H)**, in which the metal ions are arranged in ribbons and are separated by the long axis of the organic molecules, as demonstrated by X-ray powder diffraction analysis of the solids and grazing incidence X-ray diffraction analysis of the films on water. 2) Topotactic solid/gas reaction of these salts with H_2S to convert the metal ions into Q-particles of CdS or PbS embedded in the organic matrix that consists of the acids **6(H)** and **8(H)**. These hybrid materials have been characterized by X-ray photoelectron spectroscopy and transmission electron microscopy.

Keywords: oligo(phenyleneethynylene) · organic–inorganic hybrid composites · quantum particle · semiconductors · topotactic reactions

Introduction

Nanocrystallites of semiconductors and conducting metals that display quantum-size effects, referred to as quantum particles (Q-particles), are attracting great interest owing to their unique optoelectronic properties.[1–4] Recently, it was demonstrated that organization of the Q-particles in periodic patterns can lead to cooperative properties not shown by the individual components of the composite.[5–11] In recent years, different methodologies have been followed for the preparation of organized composites. Our interest has been directed towards the preparation of hybrid organic/inorganic composites, in which the semiconductor Q-particles are arranged periodically within an organic matrix.[12] Our strategy comprises two steps. First, crystals or crystalline films of organometallic salts are designed or selected such that the ions within these matrices are arranged in a given pattern. Subsequently, these solids are converted through topotactic solid/gas reactions into organized hybrid composites in which the newly formed Q-particles to some extent preserve the periodic order of the ions within the reactant matrix (Scheme 1). Furthermore, the particle size can be controlled by adjusting the length of the organic spacers that separate the layers of metal ions. This approach has been successfully applied for the preparation of hybrid materials starting from organic salts composed of aliphatic carboxylates or thiocarboxylates.[12–14]

Herein we report the preparation of hybrid composites with the monodisperse π-conjugated, rodlike compounds **6** and **8** as the organic matrices. These compounds consist of phenyleneethynylene units and bear carboxyl groups at both ends. To ensure solubility of the organic compounds, the phenylene moieties are substituted with hexyl chains. The Q-particles generated within such films are presumed to be interconnected through the molecular rods. The dicadmium **6(Cd)**, **8(Cd)** and dilead salts **6(Pb)**, **8(Pb)** of the acids **6(H)**, **8(H)** have been synthesized either in the form of crystalline powders or as thin films at the air–water interface. The crystalline powders were investigated by X-ray diffraction (XRD). The

[a] Prof. Dr. M. Lahav, Dr. V. Hensel, Dr. R. Popovitz-Biro, Dr. H. Cohen, Dr. I. Weissbuch
Department of Materials and Interfaces
The Weizmann Institute of Science, 76100 Rehovot (Israel)
Fax: (+972) 98-34-4138
E-mail: meir.lahav@weizmann.ac.il

[b] Dr. A. Godt
Max-Planck-Institut für Polymerforschung
Ackermannweg 10, 55128 Mainz (Germany)

[c] Dr. T. R. Jensen, Dr. K. Kjaer
Condensed Matter Physics and Chemistry Department
Risø National Laboratory, 4000 Roskilde (Denmark)

[d] Prof. Dr. E. Lifshitz
Department of Chemistry and Solid-State Institute
Technion-Israel Institute of Technology, 32000 Haifa
Technion City (Israel)

  0947-6539/02/0806-1413 $ 17.50+.50/0

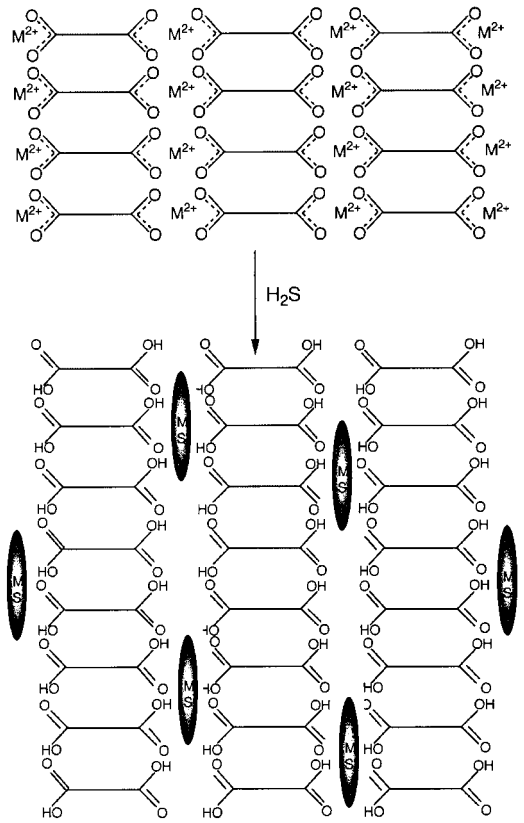

Scheme 1. Schematic representation of the conversion of the metal salts into the hybrid composites. The Q-particles formed are elongated and intercalated between the organic molecules. Note that the Q-particles and the diacids are shown on different scales; M = Cd, Pb; MS = CdS, PbS.

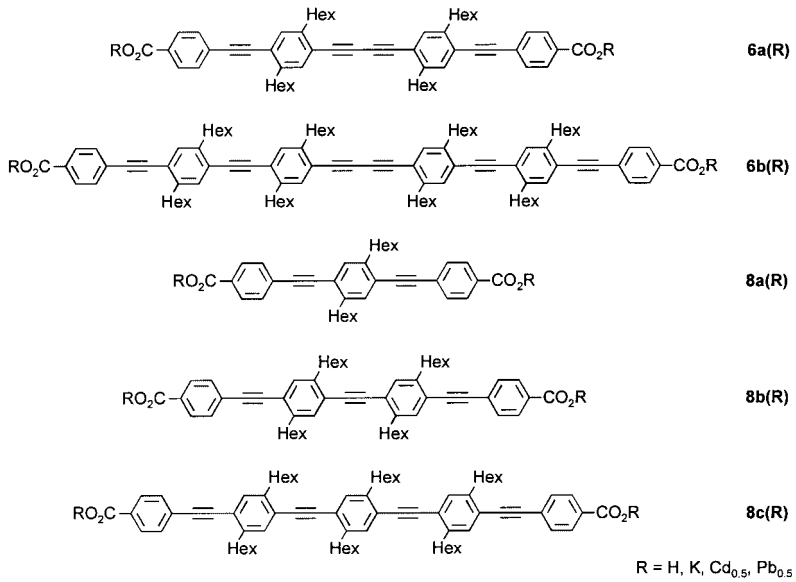

thin films were analyzed directly at the air–water interface by grazing incidence X-ray diffraction (GIXD). The cadmium and lead salts were treated with gaseous H_2S to yield, through a topotactic reaction, the corresponding hybrid materials composed of CdS or PbS Q-particles of different sizes arranged in rows and separated by the organic rods. The compositions and structures of the composites were determined by transmission electron microscopy (TEM) and X-ray photoelectron spectroscopy (XPS). Cooperative effects in the photoluminescence properties were observed for some of the composites and are presented elsewhere.[15]

Results and Discussion

Synthesis of the monodisperse rodlike dicarboxylates 6a,b(H) and 8a–c(H): The five monodisperse, rodlike dicarboxylic acids **6a,b(H)** and **8a–c(H)** were selected for the present study. Their synthesis starts from monodisperse oligo(phenyleneethynylene)s (oligoPPEs) **1** with one protected and one monosubstituted ethynylene end group (Scheme 2). Compounds **1** were prepared according to a protocol that enables the isolation of monodisperse oligoPPEs in gram amounts, as recently described by one of us.[16, 17] Because the oligoPPEs **1** decompose upon storage, they were used immediately after preparation. Coupling of the oligoPPEs **1** with methyl 4-iodobenzoate, catalyzed by $[Pd(PPh_3)_2Cl_2]$ and CuI, gave the monoesters **2**.[17] The coupling reaction was accompanied by oxidative alkyne dimerization of the oligoPPEs **1**. The resulting nonpolar butadiynes **3** could easily be separated from the polar coupling products **2** by column chromatography. However, it proved difficult to remove residual methyl 4-iodobenzoate from product **2**. Therefore, it is best to use **1** in sufficient excess to ensure that all the methyl 4-iodobenzoate is consumed. The alkyne protecting group of the monoesters **2** was cleaved by reaction with nBu_4NF. Treatment of the thus obtained deprotected monoesters **4a,b** with $[Pd(PPh_3)_2Cl_2]$ and CuI in piperidine/THF under air[18] resulted in oxidative alkyne dimerization to give the diesters **5a,b**. To obtain the diesters **7a–c**, the deprotected monoesters **4a–c** were coupled with methyl 4-iodobenzoate. The formation of the diesters **7a–c** was accompanied by some formation of diesters **5a–c** (up to 12%) due to competitive oxidative alkyne dimerization, even though methyl 4-iodobenzoate was used in huge excess. These by-products could be removed by chromatography. Saponification of the diesters **5** and **7** under basic conditions gave the diacids **6(H)**, **8(H)**, which were converted to the corresponding potassium salts **6(K)**, **8(K)**.

Preparation and characterization of the organic/inorganic hybrid composites: Crystalline powders of the cadmium and lead salts **6(Cd,Pb)**, **8(Cd,Pb)** (Schemes 1 and 2) were obtained from the corresponding potassium salts **6(K)**, **8(K)** by reaction with $CdCl_2$ or $Pb(NO_3)_2$, either under homogeneous conditions in THF/water at 40 °C or under heterogeneous conditions in ethanol/water at 40 °C. Although both methods led to quantitative cation exchange, the preparation under homogeneous conditions proved to be more convenient

0947-6539/02/0806-1414 $ 17.50+.50/0 *Chem. Eur. J.* **2002**, *8*, No. 6

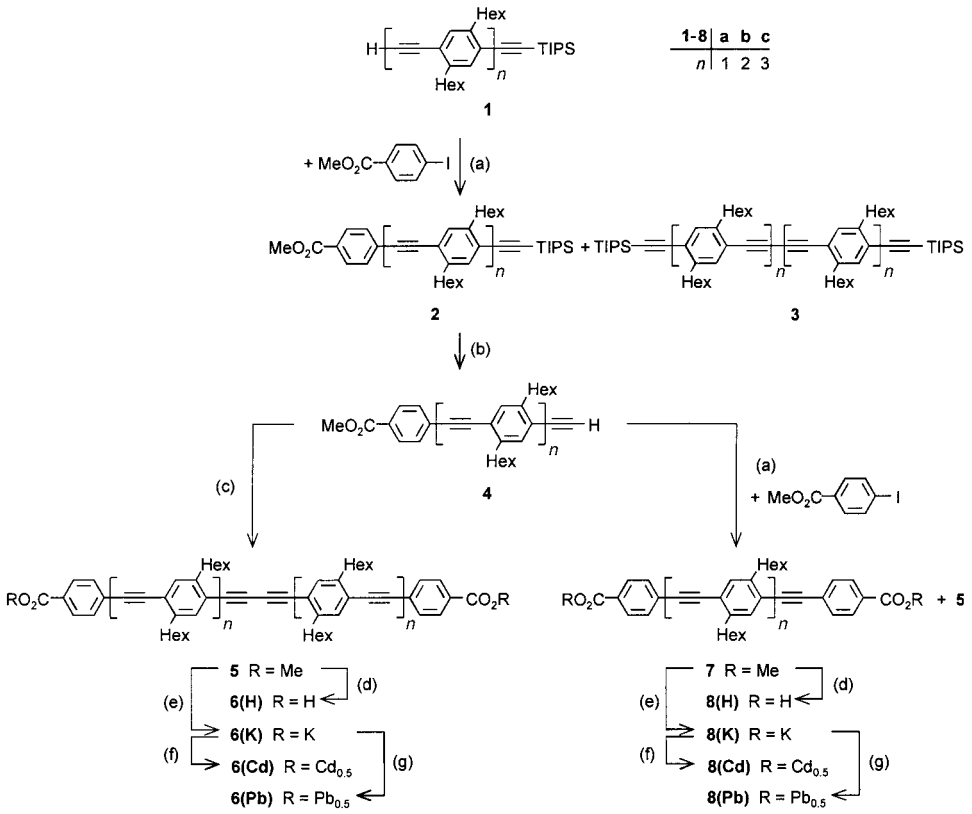

Scheme 2. a) $[PdCl_2(PPh_3)_2]$, CuI, piperidine, THF; b) nBu_4NF, THF; c) $[PdCl_2(PPh_3)_2]$, CuI, piperidine, THF, air; d) 1) KOH, methanol, THF; 2) CF_3CO_2H; e) KOH, MeOH, THF; f) $CdCl_2$, THF, H_2O; g) $Pb(NO_3)_2$, THF, H_2O.

because the reaction was faster and could easily be monitored by the precipitation of the Cd or Pb salts. Thin crystalline films of **6(Cd,Pb)**, **8(Cd,Pb)** were prepared by spreading solutions of the diacids **6(H)**, **8(H)** in chloroform or in chloroform/ethanol (9:1) on aqueous solutions of $CdCl_2$ (pH 8.5) or $Pb(NO_3)_2$. The powders and the films were exposed to H_2S at 4 °C or 25 °C at atmospheric pressure to yield the corresponding hybrid materials (Scheme 1). The reactions were quantitative within 15–60 minutes according to IR[19] and XPS spectroscopy. The dicarboxylic acids proved to be inert towards H_2S; no reaction was detected when the acids were treated with H_2S under the same conditions as the corresponding cadmium and lead salts. Furthermore, the acids could be isolated unchanged (according to TLC and ^1H NMR spectroscopy) by stirring of the hybrid composites in chloroform/ethanol (9:1).

X-ray diffraction analysis of the three-dimensional crystalline powders: The powders of the Cd and Pb salts were analyzed by XRD with the intention to obtain information on the organization of the ions within these solids. The metal ions in the salts **6a(Cd)** and **6a(Pb)** are arranged in ribbons with spacings of about 29 Å and 28 Å, respectively, as can be calculated from the (100), (200), and (300) Bragg peaks of **6a(Cd)** and the (100) and (200) Bragg peaks of **6a(Pb)**. The XRD signals of **6b(Cd)** and **6b(Pb)** are very broad, suggesting very low ordering. The salts **8a(Cd)**, **8a(Pb)** give rise to intense diffraction peaks. The (100), (200), and (300) Bragg peaks measured for **8a(Cd)** correspond to a spacing of about 22.5 Å between the ribbons of the ions. The (100) Bragg peak of **8a(Pb)** reveals a *d*-spacing of about 21.5 Å. The XRD measurement of **8c(Pb)** shows a (100) Bragg peak that corresponds to a spacing of about 32 Å. All measured spacings are smaller than the length of the rodlike diacids, suggesting that the molecules are not orthogonal to the lattice planes.

Grazing incidence X-ray diffraction analysis of thin crystalline films: It has been shown previously that amphiphilic molecules, when spread at the air–water interface, interact with metal ions present in the aqueous subphase yielding "two-dimensional" crystalline films oriented vis-à-vis the water surface through self-assembly.[20–22] The structure of these crystalline films resembles that of the three-dimensional crystals. By applying this method to the diacids **6(H)** and **8(H)**, we obtained thin films of the salts **6a(Cd)**, **6b(Cd)**, **6b(Pb)**, and **8b(Cd)** on the water surface. Their structures were determined by GIXD, which revealed structural information that could not be obtained from the XRD measurements on some of the three-dimensional powders.

The GIXD pattern obtained from diacid **6b(H)** spread on pure water for a nominal molecular area of 200 Å^2 (defined as the surface area of the trough divided by the number of molecules) displays a single Bragg peak corresponding to a *d*-spacing of 3.6 Å (Figure 1a), which is a characteristic value for the $\pi-\pi$ stacking of aromatic rings, as observed in related systems.[23] This Bragg peak is very broad, corresponding to a lateral stack size of about 25 molecules. No evidence was found for ordering in the direction of the long molecular axis or of the hexyl chains. The film thickness of about 13 Å, as determined from the Bragg rod intensity profile (Figure 1b), is consistent with there being more than a monolayer at the surface, since the hexyl chains are pointing out of the plane of the film and are disordered due to a lack of favorable contacts. Surface compression of the films to nominal molecular areas of 100 Å^2 and 70 Å^2 did not increase the degree of order.

When spread on aqueous solutions of $CdCl_2$ or $Pb(NO_3)_2$, the diacid **6b(H)** was quantitatively transformed into the corresponding salts **6b(Cd)** or **6b(Pb)**, as was proven by the absence of the Bragg peak corresponding to a *d* spacing of 3.6 Å observed when the diacid was spread on pure water.

The GIXD pattern measured from **6b(Pb)**, obtained when **6b(H)** was spread on aqueous 1 mM $Pb(NO_3)_2$ for a nominal molecular area of 200 Å^2, displays a series of four Bragg peaks

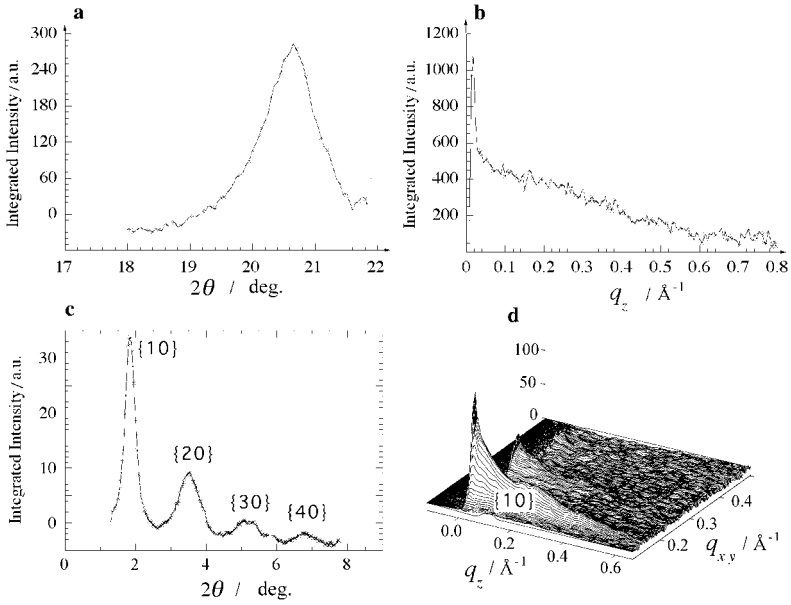

Figure 1. GIXD patterns measured from **6b(H)** spread for a nominal molecular area of 200 Å on: a) pure water, and c) on aqueous $Pb(NO_3)_2$ solution (1 mM). In a) and c), the GIXD patterns are represented as the scattered intensity $I(2\theta)$, with 2θ being the diffraction angle in degrees at the measuring wavelength of the X-ray beam, $\lambda = 1.30$ Å, integrated over the whole window of the PSD detector and showing the Break peaks. b) Bragg rod intensity profile $I(\boldsymbol{q}_z)$ in the direction perpendicular to the liquid surface and corresponding to the Bragg peak in a). d) Surface plot of the scattered intensity $I(\boldsymbol{q}_{xy},\boldsymbol{q}_z)$, where $\boldsymbol{q}_{xy}$ is the horizontal component and $\boldsymbol{q}_z$ is the vertical component of the scattering vector corresponding to the GIXD pattern shown in c).

(Figure 1c,d). These peaks correspond to a single *d*-spacing of 42 Å. Based on the calculated length of the long molecular axis of the organic rodlike molecule of 48.2 Å, we attribute the observed Bragg peaks to the *d*-spacing of a layer structure oriented parallel to the liquid surface. Within the layer, the Pb^{2+}-bound dicarboxylate salt molecules are oriented with their long molecular axes parallel to the liquid surface yielding ribbons of ions separated by ribbons of the organic rods (Scheme 1). From the deviation of the measured *d*-spacing of 42 Å from the calculated length of 48.2 Å for **6b(H)**, an angle of about 29° between the long axis of the dicarboxylate and the normal to the ribbon of metal ions is calculated. The size of the ordered domains in the direction of the long axis of the dicarboxylate is about 200 Å, corresponding to an arrangement of about five molecules of **6b(Pb)**. All the Bragg rod intensity profiles along the surface normal have maximum intensity at the horizon (Figure 1d), in agreement with the strong contribution of the Pb^{2+} ions to the measured intensity. The film was about 24 Å thick.

Analysis of the GIXD pattern yielded a model packing arrangement[24] that consists of molecules arranged by translation in a two-dimensional unit cell of dimensions $a = 48.2$ Å, $b = 4.5$ Å, $\gamma = 61°$, (Figure 2a,b). Based on calculated (*h*,*k*,0) powder diffraction patterns[24] using an atomic coordinate

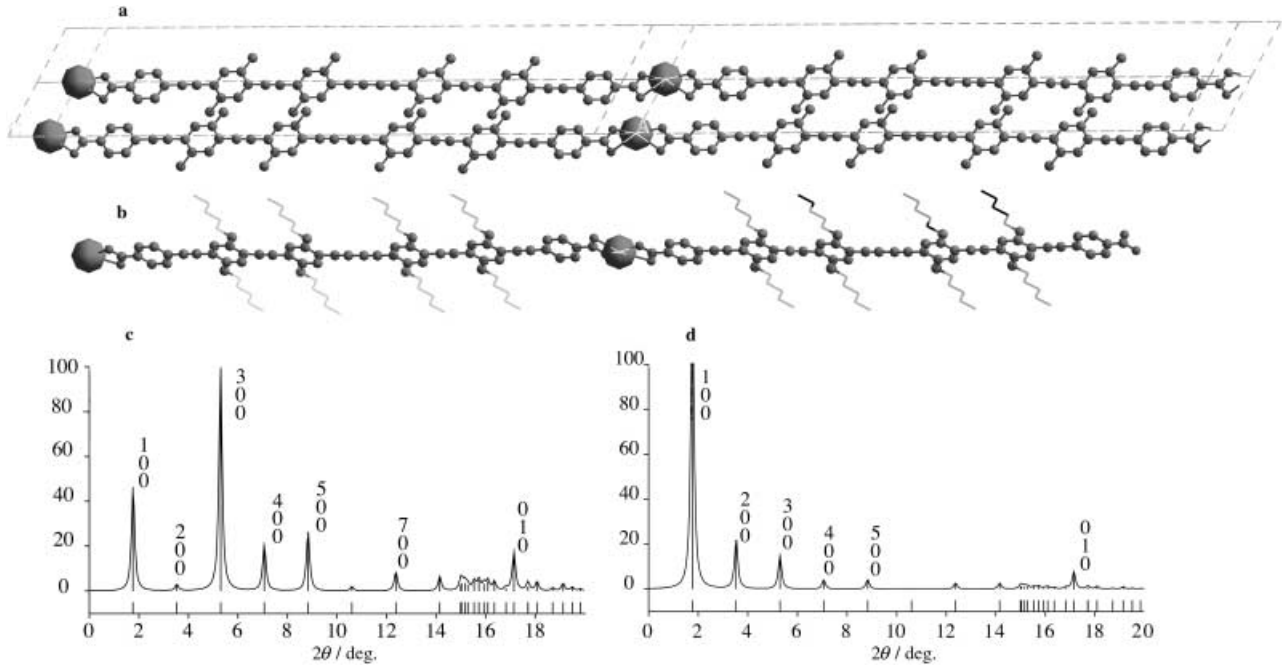

Figure 2. a) and b): Model packing arrangement of the two-dimensional film of **6b(Pb)** self-assembled at the air–solution interface: a) view perpendicular and b) view parallel to the liquid surface. Note that in a) only one C atom of the hexyl chains is shown, since it is the only one that contributes to the scattered intensity; in b), the other five C atoms of the hexyl chains, which are disordered, are drawn schematically as lines for the sake of clarity. c) and d): Calculated (*h*,*k*,0) powder diffraction patterns, $I(2\theta$ in degrees) at $\lambda = 1.30$ Å, using the atomic coordinate model shown in a) and b), but considering different contributions from the hexyl chains. In c), all six of the C atoms contribute, whereas in d) only those C atoms connected to the phenyl rings are considered.

  0947-6539/02/0806-1416 $ 17.50+.50/0 *Chem. Eur. J.* **2002**, *8*, No. 6

model, we conclude that four to five carbon atoms of the hexyl chains must be disordered and therefore do not contribute to the diffraction, thereby accounting for the observed intensity of the (*h*,0,0) Bragg peaks (Figure 2c,d). Moreover, the absence of the (010) Bragg peak in the measured GIXD pattern leads us to assume that the degree of order in the direction perpendicular to the long molecular axis is very low and that the molecules are slightly shifted from their required ideal lattice positions. Since the hexyl chains pointing out of the layer plane are disordered, the film might be more than one layer thick, with no ordering in the direction perpendicular to the water surface.

Oriented thin films of **6b(Cd)** were obtained by spreading **6b(H)** on aqueous 1 mM $CdCl_2$ (pH 8.5) for a nominal molecular area of 200 Å^2, (Figure 3a,b). The GIXD pattern, and thus the structure of **6b(Cd)**, is similar to that of **6b(Pb)**.

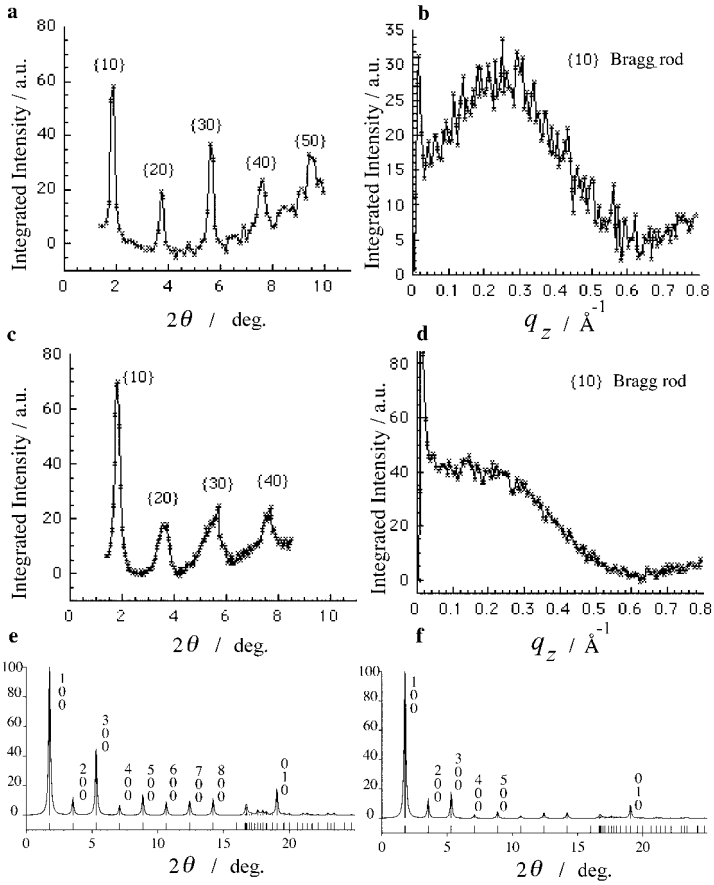

Figure 3. a)–d): GIXD patterns measured from **6b(H)** spread on a aqueous $CdCl_2$ solution (1 mM) for nominal molecular areas of 200 Å^2 (a, b) and 138 Å^2 (c, d). Note that a) and c) display the diffraction patterns as $I(2\theta)$ at $\lambda = 1.30$ Å, while b) and d) show the Bragg rod intensity profiles $I(q_z)$ corresponding to the {10} Bragg peaks of a) and c). e) and f): Calculated (*h*,*k*,0) powder diffraction patterns, $I(2\theta$ in degrees) at $\lambda =$ 1.30 Å, using an atomic coordinate model and considering different contributions from the hexyl chains. In e), all six of the C atoms contribute, whereas in f) only those C atoms connected to the phenyl rings are considered.

The different contribution of Cd^{2+} ions as compared with that of Pb^{2+} ions (46 electrons as against 80 electrons of Pb^{2+}) to the diffraction accounts for the different relative intensities of the five Bragg peaks. The five Bragg peaks of **6b(Cd)** correspond to a *d* spacing of 39 Å. Surface compression to 138 Å^2 per molecule yielded a GIXD pattern (Figure 3c,d) that shows, as indicated by the asymmetry of the Bragg peaks, the formation of two different but very similarly ordered phases with *d* spacings of 42 Å and 39 Å. The film thickness of about 14 Å is indicative of a monolayer or a bilayer, with five carbon atoms of the hexyl chains being disordered, as suggested by the simulated (*h*,*k*,0) powder diffraction patterns (Figure 3e,f).

GIXD experiments showed that the thin films of **6a(H)**, **6a(Cd)**, and **8b(Cd)** at the air–water interface have similar structures to those described for **6b(H)**, **6b(Pb)**, and **6b(Cd)**, respectively. Compound **6a(H)** spread on pure water yielded a single Bragg peak corresponding to a *d*-spacing of 3.6 Å, which is indicative of an aromatic face-to-face stacking. This spacing is identical to that observed for compound **6b(H)**. When **6a(H)** was spread on 1 mM aqueous $CdCl_2$ solution (pH 8.5) for a nominal molecular area of 120 or 100 Å^2, the GIXD pattern (Figure 4a,b) exhibited only Bragg peaks

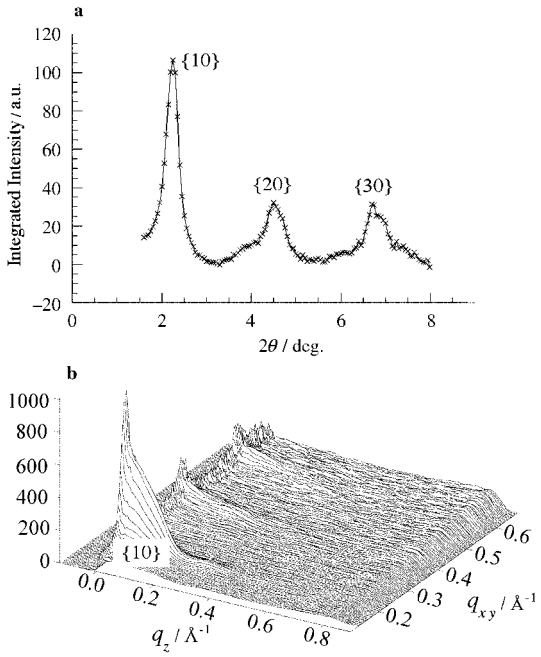

Figure 4. a) and b): GIXD patterns measured from **6a(H)** spread on a aqueous $CdCl_2$ solution (1 mM) for nominal molecular areas of 120 Å^2 and 100 Å^2; a) diffraction pattern as $I(2\theta)$ at $\lambda = 1.30$ Å, and b) the surface plot of the scattered intensity $I(q_{xy},q_z)$.

corresponding to a *d*-spacing of 33.7 Å, a value similar to the estimated length of the long molecular axis. This GIXD result implies that the self-assembled thin film of **6a(Cd)** assumes a structure similar to that of **6b(Pb)**, but with the long molecular axis perpendicular to the ribbon of metal ions (Figure 5a,b). On the basis of the calculated (*h*,*k*,0) powder diffraction patterns using an atomic coordinate model, we propose that the hexyl chains are disordered. Such disorder accounts for the observed intensities of the (*h*,0,0) Bragg peaks (Figure 5c,d). The absence of the (010) Bragg peak in the measured GIXD pattern (Figure 4) may be explained by assuming that the degree of order in the direction perpendic-

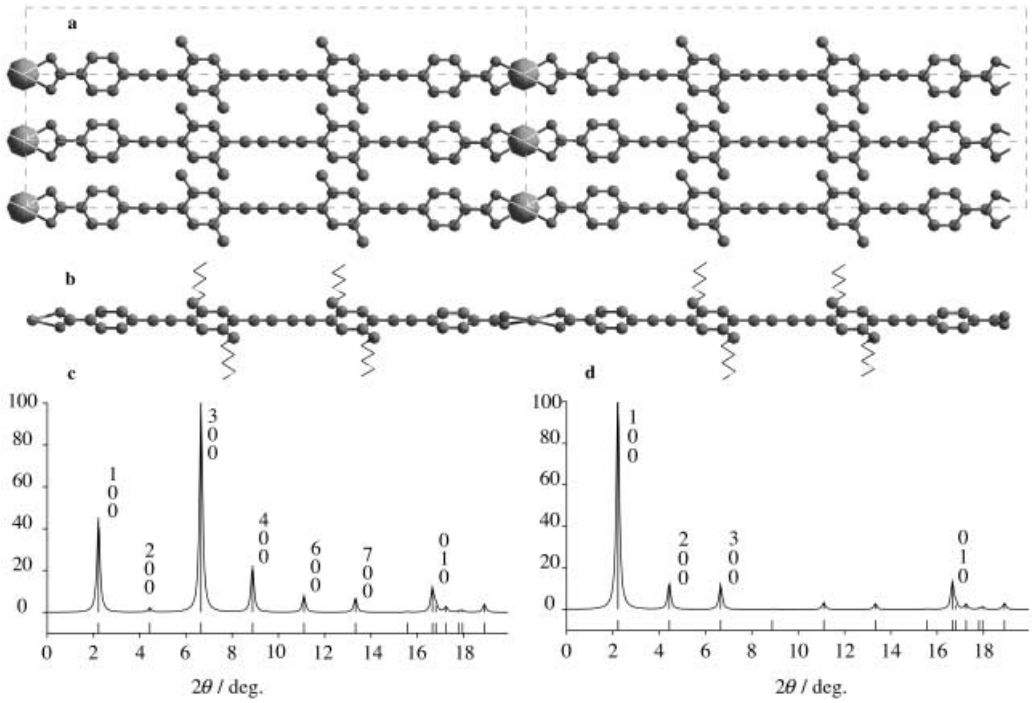

Figure 5. a) and b): Model packing arrangement of the two-dimensional film of **6a(Cd)** self-assembled at the air-solution interface: a) view perpendicular and b) view parallel to the liquid surface. Note that in a) only one C atom of the hexyl chains is shown since it is the only one that contributes to the scattered intensity; in b), the other five C atoms of the hexyl chains, which are disordered, are drawn schematically as lines for the sake of clarity. c) and d): Calculated $(h,k,0)$ powder diffraction patterns, $I(2\theta$ in degrees) at $\lambda = 1.30$ Å, using the atomic coordinate model shown in a), and b), but considering different contributions from the hexyl chains. In c), all six of the C atoms contribute, whereas in d) only those C atoms connected to the phenyl rings are considered.

ular to the long molecular axis is very low. The film thickness is about 25 Å, corresponding to more than one layer, but with no registry in the direction perpendicular to the surface due to the disorder of the hexyl chains. Surface compression does not change the GIXD pattern; it merely increases the film thickness.

A film of **8b(Cd)** was prepared by spreading the diacid **8b(H)** over an aqueous $CdCl_2$ solution (1 mM, pH 8.5) for a nominal molecular area of 200 Å^2. The GIXD pattern measured for this salt at 100 Å^2 was very weak and featured only two Bragg peaks corresponding to a single *d*-spacing of 30.6 Å. The film thickness estimated from the width of the Bragg rods was about 30 Å, implying that it corresponds to more than one layer. The degree of order of the **8b(Cd)** salt is much lower than that of the **6a(Cd)** salt.

A comparison of the layer spacings of the oriented crystalline films and those of the corresponding three-dimensional powders reveals some differences in the tilt angles of the molecules. Such differences may arise from the presence of pronounced surface effects that propagate toward the bulk of the film. Similar structural differences have been observed in the packing arrangements of α,ω-alkanediols in three-dimensional arrays and thin films crystallized at the air–water interface.[25]

X-ray photoelectron spectroscopy (XPS): The XPS spectra of all ten different salts were measured prior to reaction with H_2S. The element concentration analysis and the binding energies of the ions confirmed the 2:1 metal ion/organic matrix composition. In order to characterize the structures of the hybrid materials, representative samples were analyzed by XPS. Thus, three-dimensional crystal line powders, as well as thin films formed on the water surface and transferred to glass substrates, were measured both before and after treatment with H_2S. The chemical reaction could be identified in all the systems, as manifested in the appearance of a sulfur signal and in several line shifts similar to those reported previously.[12, 13] Table 1 lists the shifts of the metal signal (Cd, Pb) and the binding energy of the S($2p_{3/2}$) associated with the creation of Q-size nanoparticles for the hybrid matrices of compounds **6b**, **8b**, and **8c**. A split in the O(1s) line and a shift in the secondary C(1s) line arising from the carbon end group were also observed, in full agreement with previous studies.[13] The first column in Table 1 shows a systematic change in the sulfur-to-metal intensity ratio with an excess of the metal ion.

Table 1. XPS characterization of the CdS and PbS nanoparticles within the hybrid composites of compounds **6b**, **8c**, and **8b**; S^{red}/metal is the atomic concentration ratio (evaluated for the *reduced* $S(2p)$ line with respect to the *total* metal signal); $E_B(S^{red})$ is the $S(2p_{3/2})$ binding energy, given in eV; and ΔE_B(metal) is the metal line shift (in eV) upon reaction with H_2S.

	S^{red}/metal	$R/\Delta R$	$E_B(S^{red})$	ΔE_B(metal)
6b(CdS)	0.58 ± 0.02	8	161.8 ± 0.2	$0.45 \pm .0.1$
6b(PbS)	0.57 ± 0.07	8	161.0 ± 0.1	1.5 ± 0.1
8c(CdS)	0.73 ± 0.03	16	161.7 ± 0.1	0.45 ± 0.1
8c(PbS)	0.71 ± 0.05	15	160.8 ± 0.1	1.5 ± 0.1
8b(CdS)	0.85 ± 0.1	34	161.6 ± 0.1	0.45 ± 0.1
8b(PbS)	0.75 ± 0.1	18	160.6 ± 0.1	1.5 ± 0.1

0947-6539/02/0806-1418 $ 17.50+.50/0 *Chem. Eur. J.* **2002**, *8*, No. 6

Ideally, this ratio would be expected to be unity in CdS or PbS particles, hence deviations may be related to particle surface signals. We therefore assume that the reduced signal intensity for sulfur arises only from the particle core, and we attribute all extra intensity of the metal signals to the particle shell. In fact, the Pb shifts are sufficiently large to support this argument, showing a resolved shoulder attributable to oxidized material, which corresponds precisely to the additional amount of Pb (relative to the reduced amount of sulfur). This oxidized Pb shoulder appears at a binding energy about 0.3 eV lower than that of the unreacted Pb, similar to that previously reported in an earlier study.[13] Hence, a medium oxidation state for the shell Pb atoms is more than expected, owing to the presence of surrounding matrix oxygen atoms. Based on intensity ratios, we suggest that a similar shell is likewise created on the CdS particles, although the surface Cd signal is not resolved (a consequence of considerably lower shifts of Cd as compared with Pb).

To illustrate the size estimation, one can assume a spherical shape. The core signal is given by $2I_S$ (I_S is the intensity of the reduced sulfur only) and the shell signal is given by the extra amount of the metal. The particle radius is given by $R = 6\Delta R/[I_M/(I_S - 1)]$, where I_M/I_S is the intensity ratio of the signals due to the total amount of the metal and the reduced sulfur, and ΔR is the shell thickness. The values obtained from the above expression are scaled with ΔR, yet provide a clear systematic change in R for the various matrices. We stress here that the above results also hold for the longest dicarboxylates, for which no observable evidence for the creation of the Q-particles was provided by the TEM measurements.

Transmission electron microscopy (TEM): In order to glean information on the size and organization of the CdS and PbS particles within the different organic matrices, the hybrid composites were analyzed by TEM. Powders of the composites were dispersed in an appropriate solvent and deposited on electron microscope grids. TEM images of PbS particles generated from compound **8a(Pb)** are shown in Figure 6a. The particles are spherical in shape and are randomly distributed in the organic matrix. High-resolution TEM (HRTEM) imaging of the particles, as shown in the inset of Figure 6a, was only possible after the organic matrix had been dissolved by adding small amounts of thioethanol as a capping agent followed by chloroform. The particle diameters range from 5 to 8 nm. According to electron diffraction measurements, the particles are of the cubic polymorph. Similar results were obtained for the CdS particles generated from compound **8a(Cd)**.

An image of a crystal of **6a(Pb)** after treatment with H_2S is shown in Figure 7a. This crystal preserved its morphology during the topotactic reaction with H_2S. Layers of high-contrast particles showing a periodicity of about 2.1 nm were visible in several regions along the composite crystal. Particles of 3–4 nm in diameter were imaged with high resolution (see inset) after dissolution of the organic matrix. A TEM image of a hybrid crystal of CdS in compound **6a(H)** is shown in Figure 7b. The CdS particles show a tendency to arrange in layers, but no clear periodicity could be assigned from the images. The size of the particles was determined as 2.5–3.0 nm by HRTEM after extraction (see inset).

In contrast to the above systems, CdS and PbS could not be visualized in situ in the hybrid crystals of compound **6b(H)**, although XPS and IR measurements were indicative of their formation. The existence of the Q-particles could be demonstrated and their size measured (2–3 nm) by HRTEM imaging only after dissolution of the organic matrix.

After treatment with H_2S, crystals of **8b(Pb)** show a needlelike morphology (Figure 6b). Small, elongated particles arranged along the long axis of the crystals could be observed. Particles with an average diameter of 3–4 nm were imaged

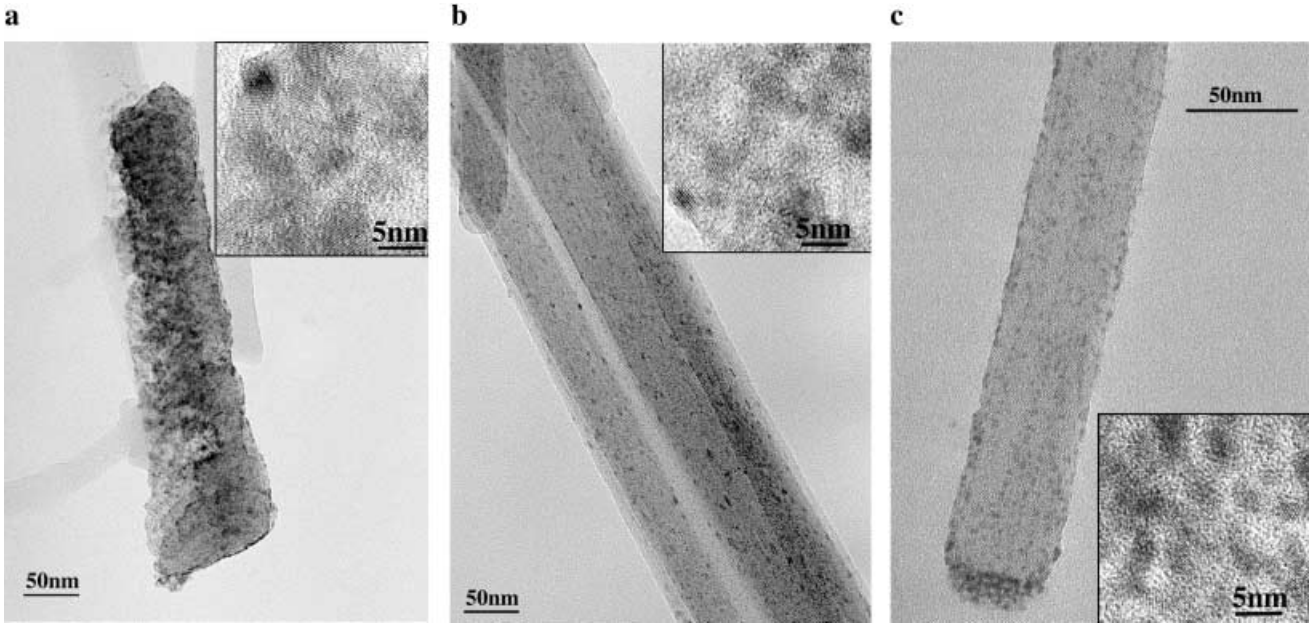

Figure 6. TEM micrographs showing hybrid crystals generated from a) **8a(Pb)**, b) **8b(Pb)**, and c) **8c(Pb)**. The insets show high-resolution images of the corresponding nanoparticles after dissolution of the organic matrices.

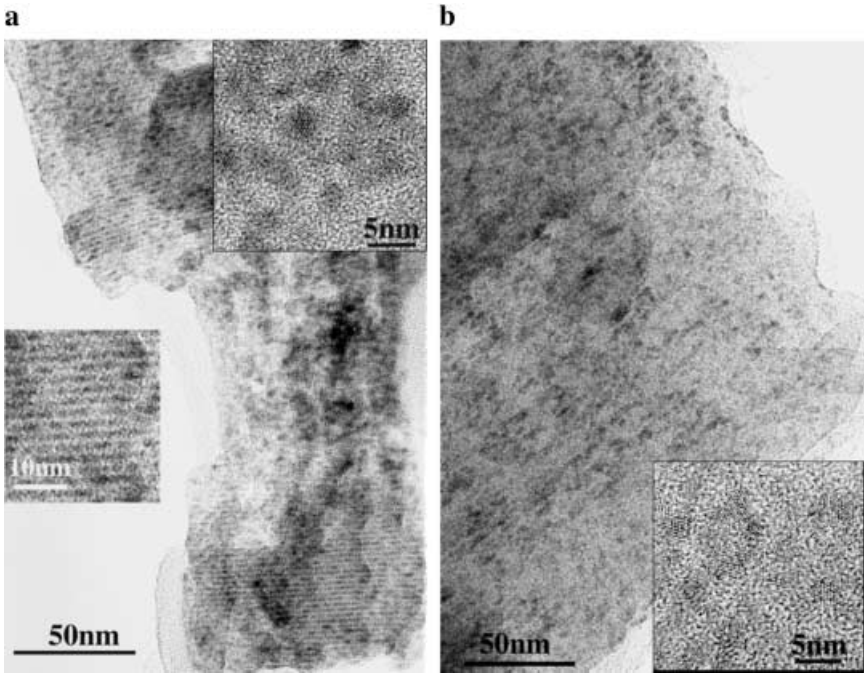

Figure 7. a) TEM micrograph of a hybrid crystal generated from compound **6a(Pb)**. One inset (left) is an enlargement of a region showing the arrangement of the PbS particles in rows. The other inset (top) shows a high-resolution image of the PbS particles after dissolution of the organic matrix. b) TEM micrograph of a hybrid crystal generated from compound **6a(Cd)**. The inset shows a high-resolution image of the CdS nanoparticles after dissolution of the organic matrix.

with high resolution (see inset) after dissolution of the organic matrix.

PbS particles embedded in hybrid crystals of compound **8c(H)** were not detected as formed in situ, but only became visible after etching of the organic crystal through partial dissolution of the matrix with chloroform (Figure 6c). After complete dissolution of the organic matrix, particles of average size 2–3 nm could be imaged by HRTEM, as shown in the inset. CdS particles with an average size of 3–4 nm could be observed by HRTEM within the elongated crystals of **8c(Cd)** after treatment with H_2S.

Conclusion

Topotactic solid/gas reactions have been successfully applied for the preparation of ordered hybrid composites made up of monodisperse, fully conjugated, rodlike molecules and semiconductor Q-particles of CdS and PbS, arranged in periodic rows. The new composites preserve the morphological integrity of the reactant phase. The size of the Q-particles formed is dependent on the spacing between the metal ions in the reactant matrix prior to reaction. Furthermore, in the systems **8a(Cd)** and **8a(Pb)**, in which the length of the rods, and thus the spacing between the rows of ions, is about 2 nm, the Q-particles formed after reaction with H_2S are spherical, 5–8 nm in diameter, and are randomly deposited throughout the organic matrix. On the other hand, when the rodlike molecules are longer, such as 2.6–4.3 nm, the generated Q-particles are elongated and embedded within the organic matrix. This trend is in accordance with previously reported results on aliphatic systems.[12–14] Consequently, the detection of the particles in these composites only becomes possible after partial dissolution of the matrix, or after their complete extraction.

Preliminary spectroscopic studies on some of the composites have indicated efficient energy transfer from the organic rods to the Q-particles. Furthermore, a red shift in the wavelength of the photoluminescence emission of the Q-particles embedded in the solid matrices demonstrates the existence of cooperative effects originating from strong coupling between the Q-particles and the organic rods.[15] The present synthetic methodology is currently being applied to the preparation of other ordered composites, in particular hybrids in the form of single crystals, which are expected to display anisotropic optical properties.

The present method may also be applicable for the preparation of hybrid thin organic films for coating optoelectronic devices.

Experimental Section

Physical characterization: XPS measurements were performed on a Kratos Analytical AXIS-HS set-up, with a monochromated $Al_{K\alpha}$ source ($h\nu$ = 1486.6 eV) and pass energies ranging from 20 to 80 eV. Charge compensation was used in all measurements, while final energy scale calibration was determined by setting the main carbon line to 284.7 eV. In order to eliminate beam-induced damage,[26] time evolution of the signals was studied by repeatedly scanning at a fixed spot and comparing this with rapid scans on fresh areas. In general, no spectroscopic evidence of damage could be detected on a time scale of 1–2 hours, though visually slight color changes were observed on the three-dimensional crystals within about 5 minutes.

Sample exposure to air was normally limited to 5 minutes or less. Longer exposures were used to study the role of instability upon air exposure, observed visually on time scales of hours to days, depending on the host matrix.

TEM images and electron diffraction patterns were obtained on a Philips CM 120 transmission electron microscope operated at 120 kV.

XRD measurements were performed on a Rigaku RU-200B Rotaflex diffractometer with $Cu_{K\alpha}$ radiation, λ = 1.54 Å, operated at 50 mV, 150 mA.

The grazing incidence X-ray diffraction technique (GIXD), a surface-sensitive, in situ analytical method for Langmuir monolayers, is described in detail elsewhere.[22] The GIXD experiments were carried out at the beamline BW1 using the liquid surface diffractometer at the Hasylab synchrotron source, DESY, Hamburg. The samples were prepared by spreading the solutions [$\sim 5.0 \times 10^{-4}$ M in chloroform or a mixture of chloroform and ethanol (9:1)] of the diacids **6(H)**, **8(H)** on water and on aqueous 1 mM $CdCl_2$ (pH 8.5) or 1 mM $Pb(NO_3)_2$ at 20 °C. Oriented multilayer films of the corresponding metal salts spontaneously self-assembled at the air–solution interface. The trough, mounted on the diffractometer and equipped with a Wilhelmy balance, was sealed, flushed with helium and equilibrated at 5 °C for 1 hour.

The GIXD patterns were measured by scanning over a range along the horizontal component of the X-ray scattering vector, $\boldsymbol{q}_{xy} \approx (4\pi/\lambda)\sin\theta_{xy}$), $2\theta_{xy}$ being the horizontal scattering angle defined by a Soller collimator.

0947-6539/02/0806-1420 $ 17.50+.50/0 *Chem. Eur. J.* **2002**, *8*, No. 6

The scattered intensity was measured with a position-sensitive detector (PSD), which resolved the vertical component of the X-ray scattering vector, $q_z \approx (2\pi/\lambda)\sin\alpha_f$ (where α_f is the angle between the diffracted beam and the horizon), in the q_z range 0.00 to 1.20 Å^{-1}. The diffraction data may be presented in three ways: 1) the GIXD pattern as a two-dimensional intensity distribution $I(q_{xy},q_z)$ in a surface or contour plot; 2) the GIXD pattern $I(q_{xy})$ obtained by integrating over the whole q_z window of the PSD, which yields the Bragg peaks; 3) the Bragg rod intensity profiles, which are the scattered intensity $I(q_z)$ recorded in channels along the PSD integrated across the q_{xy} range of each Bragg peak. Several different types of information can be extracted from the measured GIXD pattern. The $2\theta_{xy}$ (or q_{xy}) positions of the Bragg peaks were used for the calculation of the lattice repeat distances $d = 2\pi/q_{xy}$ and assigning them {*h*,*k*} Miller indices yielded the unit cell parameters. The vertical full-width at half-maximum, FWHM(q_z), of the Bragg rod intensity profiles gave an estimate of the thickness $d \approx 0.9(2\pi/\mathrm{FWHM}(q_z))$ of the crystalline film on the water surface. The horizontal full-width at half-maximum of the Bragg peaks FWHM(q_{xy}) yielded the crystalline coherence lengths $L_{hk} \approx 0.9(2\pi/\mathrm{FWHM}(q_{xy}))$. Molecular modeling was performed using the Cerius^2 program package.[24]

General: All chemicals were purchased from Aldrich. THF was distilled from sodium/benzophenone. Piperidine was dried by refluxing over CaH_2. The petroleum ether used had a boiling range of 40–60 °C. For chromatography, Merck silica gel (0.040–0.063 mm; 230–400 mesh) was used. TLC was carried out on silica gel coated aluminum foils (Merck aluminum foils $60F_{254}$). Unless otherwise stated, NMR spectra were recorded from samples in $CDCl_3$ on a 250 MHz spectrometer at room temperature. Residual $CHCl_3$ served as an internal standard. FT-IR spectra were obtained on a Nicolet 460 spectrometer from samples in KBr pellets. UV/Vis spectra were recorded from solutions of the samples in $CHCl_3$/methanol (9:1) on a Perkin–Elmer spectrophotometer. The concentrations used were in the range 10^{-5}–10^{-6} mol dm^{-3}. Melting points were determined on a Fisher–John melting point apparatus.

General procedure for the alkynyl–aryl coupling: The reactions were carried out under argon. $[Pd(PPh_3)_2Cl_2]$ (1 mol% with respect to the aryl halide) and CuI (2 mol% with respect to the aryl halide) were added to a degassed solution of the two coupling components in THF/piperidine at room temperature. Shortly thereafter, a precipitate formed. After stirring the reaction mixture for 10–18 h at room temperature, the solvents were evaporated. The residue was redissolved in diethyl ether and the organic phase was washed with water until the aqueous phase stayed neutral. The organic phase was then dried ($MgSO_4$) and the solvent was evaporated. The product was isolated by column chromatography. In the case of **2**, the nonpolar butadiyne **3** formed as a by-product was eluted with hexane in a first fraction. The alkynyl–aryl coupling products **2** were then isolated by switching the eluent to hexane/ethyl acetate, 10:1.

TIPS-protected monoester 2a: Reaction of **1a**[16] (6.69 g, 14.8 mmol) with methyl 4-iodobenzoate (3.53 g, 13.5 mmol) in THF (180 mL) and piperidine (60 mL) for 14 h gave **2a** (7.3 g, 93%) as a colorless oil. $R_f = 0.55$ (hexane/ethyl acetate, 10:1); ^{1}H NMR: $\delta = 8.03$ and 7.56 (AA′XX′, 2H each; ArH of benzoate ring), 7.33 (s, 1H; ArH), 7.31 (s, 1H; ArH), 3.93 (s, 3H; OCH_3), 2.82–2.71 (m, 4H; ArCH_2), 1.66–1.57 (m, 4H; ArCH_2CH_2), 1.39–1.27 (m, 12H; CH_2), 1.15 (apparent s, 21H; TIPS), 0.91–0.84 (m, 6H; CH_2CH_3); ^{13}C NMR: $\delta = 166.4$, 142.6, 142.3, 133.0, 132.4, 131.3, 129.5, 129.3, 128.2, 123.3, 121.9, 105.5, 95.5, 92.9, 91.5, 52.1, 34.4, 34.1, 31.8, 31.7, 30.82, 30.78, 29.33, 29.26, 22.6, 18.7, 14.1, 11.3; elemental analysis calcd (%) for $C_{39}H_{56}O_2Si$ (584.96): C 80.08, H 9.65; foun:d C 79.77, H 9.81.

TIPS-protected monoester 2b: Reaction of **1b**[16] (2.10 g, 2.92 mmol) with methyl 4-iodobenzoate (695 mg, 2.65 mmol) in THF (80 mL) and piperidine (40 mL) for 15 h gave **2b** (2.0 g, 89%) as a highly viscous yellow oil. $R_f = 0.58$ (hexane/ethyl acetate, 10:1); ^{1}H NMR: $\delta = 8.02$ and 7.57 (AA′XX′, 2H each; ArH of benzoate ring), 7.37 (s, 1H; ArH), 7.35 (s, 1H; ArH), 7.31 (s, 1H; ArH), 7.30 (s, 1H; ArH), 3.92 (s, 3H; OCH_3), 2.84–2.72 (m, 8H; ArCH_2), 1.75–1.58 (m, 8H; ArCH_2CH_2), 1.39–1.25 (m, 24H; CH_2), 1.14 (apparent s, 21H; TIPS), 0.89–0.84 (m, 12H; CH_2CH_3); ^{13}C NMR: $\delta = 166.5$, 142.6, 142.5, 142.0, 141.8, 132.9, 132.5, 132.44, 132.39, 131.3, 129.6, 129.5, 128.2, 123.4, 122.9, 122.7, 121.9, 105.7, 95.4, 93.3, 93.1, 92.7, 91.6, 52.2, 34.4, 34.2, 31.8, 31.7, 30.9, 30.8, 30.7, 30.6, 29.4, 29.32, 29.25, 22.7, 22.64, 22.61, 18.7, 14.1, 11.4; elemental analysis calcd (%) for $C_{59}H_{84}O_2Si$ (853.40): C 83.04, H 9.92; found: C 82.87, H 9.98.

TIPS-protected monoester 2c: Coupling of **1c**[16] (4.00 g, 4.05 mmol) with methyl 4-iodobenzoate (1.52 g, 5.80 mmol) in THF (150 mL) and piperidine (40 mL) for 12 h gave **2c** (3.5 g, 78%) as a green-yellow solid. $R_f = 0.59$ (hexane/ethyl acetate, 10:1); m.p. 76 °C; ^{1}H NMR: $\delta = 8.04$ and 7.58 (AA′XX′, 2H each; ArH of benzoate ring), 7.39 (s, 1H; ArH), 7.38 (s, 1H; ArH), 7.36 (s, 2H; ArH), 7.32 (s, 1H; ArH), 7.31 (s, 1H; ArH), 3.94 (s, 3H; OCH_3), 2.85–2.71 (m, 12H; ArCH_2), 1.74–1.61 (m, 12H; ArCH_2CH_2), 1.45–1.28 (m, 36H; CH_2), 1.15 (apparent s, 21H; TIPS), 0.92–0.84 (m, 18H; CH_2CH_3); ^{13}C NMR: $\delta = 166.3$, 142.6, 142.4, 141.8, 141.7, 132.8, 132.4, 131.2, 129.5, 129.4, 128.4, 123.4, 122.9, 122.8, 122.7, 121.9, 105.8, 95.1, 93.4, 93.1, 92.9, 91.5, 52.0, 34.5, 34.2, 31.84, 31.76, 30.9, 30.8, 30.7, 29.3, 22.7, 18.7, 14.1, 11.4; elemental analysis calcd (%) for $C_{79}H_{112}O_2Si$ (1121.84): C 84.58, H 10.06; found: C 84.62, H 10.11.

Diester 7a: Reaction of **4a** (3.00 g, 7.00 mmol) with methyl 4-iodobenzoate (3.67 g, 14.00 mmol) in THF (100 mL) and piperidine (35 mL) gave, after chromatographic work-up (hexane/ethyl acetate, 6:1; $R_f = 0.36$), **7a** (3.4 g, 85%) as a colorless solid. Traces of the alkyne dimerization product **5a** were eluted together with some **7a** in a first fraction. Characterization of **7a**: m.p. 120 °C; ^{1}H NMR: $\delta = 8.00$ and 7.53 (AA′XX′, 4H each; ArH of benzoate rings), 7.35 (s, 2H; ArH), 3.90 (s, 6H; OCH_3), 2.84–2.74 (m, 4H; ArCH_2), 1.74–1.61 (m, 4H; ArCH_2CH_2), 1.51–1.22 (m, 12H; CH_2), 0.89–0.80 (m, 6H; CH_2CH_3); ^{13}C NMR: $\delta = 166.4$, 142.4, 132.4, 131.3, 129.4, 128.1, 122.3, 93.3, 91.5, 52.1, 34.0, 31.7, 30.6, 29.3, 22.6, 14.1; elemental analysis calcd (%) for $C_{38}H_{42}O_4$ (562.75): C 81.11, H 7.52; found: C 80.97, H 7.72; UV/Vis: λ_{max} (ε) = 346 nm (53.49×10^6 cm^{2}mol^{-1}).

Diester 7b: Reaction of **4b** (1.50 g, 2.15 mmol) with methyl 4-iodobenzoate (2.83 g, 10.8 mmol) in THF (30 mL) and piperidine (10 mL) gave, after chromatographic work-up (hexane/ethyl acetate, 1:1 → CH_2Cl_2; R_f(**7b**) = 0.69 (CH_2Cl_2), R_f(**5b**) = 0.75 (CH_2Cl_2)), **7b** (1.4 g, 79%) as a yellow solid and the alkyne dimerization product **5b** (105 mg, 7%) as a green-yellow solid. Characterization of **7b**: m.p. 115 °C; ^{1}H NMR: $\delta = 8.01$ and 7.55 (AA′XX′, 4H each; ArH of benzoate rings), 7.36 (s, 2H; ArH), 7.35 (s, 2H; ArH), 3.91 (s, 3H; OCH_3), 2.82–2.76 (m, 8H; ArCH_2), 1.73–1.62 (m, 8H; ArCH_2CH_2), 1.44–1.25 (m, 24H; CH_2), 0.88–0.83 (m, 12H; CH_2CH_3); ^{13}C NMR: $\delta = 166.5$, 142.5, 142.0, 132.54, 132.45, 131.3, 129.6, 129.4, 128.2, 123.3, 122.0, 93.2, 91.5, 52.2, 34.2, 31.9, 31.8, 30.8, 30.7, 29.3, 22.7, 14.1; elemental analysis calcd (%) for $C_{58}H_{70}O_4$ (831.19): C 83.81, H 8.49; found: C 83.58, H 8.42; UV/Vis: λ_{max} (ε) = 360 nm (87.65×10^6 cm^{2}mol^{-1}).

Diester 7c: Reaction of **4c** (3.26 g, 3.38 mmol) and methyl 4-iodobenzoate (4.43 g, 16.9 mmol) in THF (80 mL) and piperidine (20 mL) gave, after chromatographic workup (CH_2Cl_2), the alkyne dimerization product **5c** (391 mg, 12%; $R_f = 0.80$) and **7c** (2.6 g, 71%; $R_f = 0.71$), both as green-yellow solids.

Characterization of 7c: M.p. 139 °C; ^{1}H NMR: $\delta = 8.02$ and 7.56 (AA′XX′, 4H each; ArH of benzoate rings), 7.37 (s, 2H; ArH), 7.36 (s, 4H; ArH), 3.92 (s, 6H; OCH_3), 2.84–2.71 (m, 12H; ArCH_2), 1.78–1.62 (m, 12H; ArCH_2CH_2), 1.45–1.23 (m, 36H; CH_2), 0.98–0.82 (m, 18H; CH_2CH_3); ^{13}C NMR: $\delta = 166.4$, 142.4, 141.92, 141.91, 132.4, 131.3, 129.5, 129.4, 128.1, 123.3, 122.8, 121.9, 93.3, 93.1, 93.0, 91.5, 52.1, 34.1, 31.8, 31.7, 30.7, 30.6, 29.3, 22.6, 14.1; elemental analysis calcd (%) for $C_{78}H_{98}O_4$ (1099.65): C 85.20, H 8.98; found: C 85.03, H 8.87; UV/Vis: λ_{max} (ε) = 372 nm (98.81×10^6 cm^{2}mol^{-1}).

Characterization of 5c: M.p. 162 °C; ^{1}H NMR: $\delta = 8.04$ and 7.58 (AA′XX′, 4H each; ArH of benzoate rings), 7.39 (s, 4H; ArH), 7.37 (s, 6H; ArH), 7.36 (s, 2H; ArH), 3.94 (s, 6H; OCH_3), 2.91–2.71 (m, 24H; ArCH_2), 1.78–1.61 (m, 24H; ArCH_2CH_2), 1.47–1.22 (m, 72H; CH_2), 0.98–0.81 (m, 36H; CH_2CH_3); ^{13}C NMR: $\delta = 166.5$, 143.7, 142.5, 142.0, 133.3, 132.4, 131.3, 129.6, 129.4, 128.2, 123.7, 123.4, 122.8, 122.7, 121.9, 121.2, 93.7, 93.3, 93.1, 93.0, 92.9, 91.5, 81.8, 78.4, 52.2, 34.2, 34.0, 31.8, 31.7, 31.6, 30.7, 30.6, 30.5, 29.7, 29.3, 29.1, 22.6, 14.1; elemental analysis calcd (%) for $C_{140}H_{73}O_2$ (1929.01): C 87.17, H 9.51; found: C 86.96, H 9.23; UV/Vis: λ_{max} (ε) = 385 nm (183.32×10^6cm^{2}mol^{-1}).

General procedure for the removal of the TIPS group: A 1M solution of nBu$_4$NF in THF (1.1 equivalents) was added at room temperature to a degassed solution of the respective TIPS-protected ester **2a–c** in THF. The mixture was stirred for 0.5 h and then the solvent was evaporated. The residue was partitioned between diethyl ether and water. The organic phase was thoroughly washed with water, and the combined aqueous phases were extracted with diethyl ether. Finally, the combined organic phases were washed twice with water and dried ($MgSO_4$). The solvent was removed and

the product was isolated by column chromatography (hexane/ethyl acetate, 10:1). The product was used immediately for further reactions.

Deprotected monoester 4a: Starting from **2a** (6.00 g, 10.3 mmol) in THF (250 mL), **4a** (4.1 g, 93%) was obtained as a red oil. $R_f = 0.50$; ^{1}H NMR: $\delta = 8.01$ and 7.54 (AA′XX′, 2H each; ArH of benzoate ring), 7.33 (s, 1H; ArH), 7.32 (s, 1H; ArH), 3.90 (s, 3H; OCH_3), 3.32 (s, 1H; C≡CH), 2.80–2.69 (m, 4H; ArCH_2), 1.72–1.62 (m, 4H; ArCH_2CH_2), 1.41–1.30 (m, 12H; CH_2), 0.92–0.85 (m, 6H; CH_2CH_3); ^{13}C NMR: $\delta = 166.3$, 142.7, 132.9, 132.2, 131.2, 129.4, 129.3, 128.0, 122.3, 121.9, 93.0, 91.1, 82.2, 81.7, 52.0, 34.0, 33.7, 31.61, 31.55, 30.5, 30.4, 29.1, 29.0, 22.5, 17.6, 14.0; elemental analysis calcd (%) for $C_{30}H_{36}O_2Si$ (428.61): C 84.07, H 8.47; found: C 83.82, H 8.53.

Deprotected monoester 4b: Starting from **2b** (1.85 g, 2.17 mmol) in THF (50 mL), **4b** (1.4 g, 91%) was obtained as a slightly red, highly viscous oil. $R_f = 0.52$; ^{1}H NMR: $\delta = 8.02$ and 7.55 (AA′XX′, 2H each; ArH of benzoate), 7.36 (s, 1H; ArH), 7.34 (s, 1H; ArH), 7.31 (s, 2H; ArH), 3.92 (s, 3H; OCH_3), 3.29 (s, 1H; C≡CH), 2.83–2.68 (m, 8H; ArCH_2), 1.74–1.57 (m, 8H; ArCH_2CH_2), 1.40–1.35 (m, 24H; CH_2), 0.92–0.81 (m, 12H; CH_2CH_3); ^{13}C NMR: $\delta = 166.4$, 142.7, 142.4, 141.9, 141.8, 132.9, 132.5, 132.4, 131.3, 129.5, 129.4, 128.1, 123.3, 123.2, 121.9, 121.4, 93.1, 93.0, 92.8, 91.5, 82.4, 81.5, 52.1, 34.12, 34.06, 33.8, 31.8, 31.7, 31.6, 30.7, 30.6, 30.5, 29.2, 29.1, 22.6, 17.8, 17.7, 17.6, 14.0; elemental analysis calcd (%) for $C_{50}H_{64}O_2Si$ (697.05): C 86.15, H 9.25; found: C 85.89, H 9.21.

Deprotected monoester 4c: Starting from **2c** (3.50 g, 3.12 mmol) in THF (120 mL), **4c** (2.9 g, 96%) was obtained as a green-yellow solid. $R_f = 0.54$; m.p. 63 °C; ^{1}H NMR: $\delta = 8.04$ and 7.58 (AA′XX′, 2H each; ArH of benzoate ring), 7.39 (s, 1H; ArH), 7.38 (s, 1H; ArH), 7.37 (s, 2H; ArH), 7.34 (s, 2H; ArH), 3.94 (s, 3H; OCH_3), 3.30 (s, 1H; C≡CH), 2.85–2.67 (m, 12H; ArCH_2), 1.74–1.62 (m, 12H; ArCH_2CH_2), 1.44–1.31 (m, 36H; CH_2), 0.92–0.84 (m, 18H; CH_2CH_3); ^{13}C NMR: $\delta = 166.3$, 142.7, 142.4, 141.8, 141.7, 132.9, 132.4, 131.2, 129.5, 129.3, 128.1, 123.4, 123.3, 122.8, 122.7, 121.9, 121.4, 93.3, 93.1, 93.0, 92.9, 92.8, 91.5, 82.4, 81.5, 52.1, 34.2, 33.8, 31.8, 31.7, 30.7, 30.5, 29.29, 29.25, 29.1, 22.6, 14.0; elemental analysis calcd (%) for $C_{70}H_{92}O_2Si$ (965.50): C 87.08, H 9.60; found: C 86.89, H 9.86.

General procedure for the oxidative alkyne dimerizations: A mixture of the respective alkyne **4a**,**b**, $[Pd(PPh_3)_2Cl_2]$ (1 mol%), and CuI (2 mol%) in THF/piperidine was stirred overnight at room temperature under air.[18] The solvents were then evaporated, and the residue was redissolved in diethyl ether. The organic phase was washed with water until the aqueous phase stayed neutral. The organic phase was dried ($MgSO_4$) and the solvent was evaporated. The product was isolated by chromatography (hexane/ethyl acetate, 10:1).

Diester 5a: Starting from **4a** (6.00 g, 14.0 mmol) in THF (150 mL) and piperidine (20 mL), compound **5a** (4.53 g, 76%) was obtained as a green-yellow solid. $R_f = 0.28$; m.p. 120 °C; ^{1}H NMR: $\delta = 8.04$ and 7.57 (AA′XX′, 4H each; ArH of benzoate rings), 7.38 (s, 2H; ArH), 7.37 (s, 2H; ArH), 3.94 (s, 6H; OCH_3), 2.84–2.71 (m, 8H; ArCH_2), 1.77–1.60 (m, 8H; ArCH_2CH_2), 1.47–1.24 (m, 24H; CH_2), 0.95–0.82 (m, 12H; CH_2CH_3); ^{13}C NMR: $\delta = 166.2$, 143.6, 142.4, 133.2, 132.3, 131.2, 129.4, 127.9, 122.8, 121.6, 93.7, 91.1, 81.6, 78.5, 52.0, 34.0, 33.9, 31.64, 31.57, 30.4, 29.1, 29.0, 22.5, 14.0; elemental analysis calcd (%) for $C_{60}H_{70}O_4$ (855.21): C 84.27, H 8.25; found: C 84.57, H 8.36; UV/Vis: λ_{max} (ε) = 365 nm (91.79×10^6 cm^{2}mol^{-1}).

Diester 5b: Starting from **4b** (1.30 g, 1.86 mmol) in THF (40 mL) and piperidine (8 mL), **5b** (1.05 g, 81%) was obtained as a green-yellow solid. $R_f = 0.33$; m.p. 127 °C; ^{1}H NMR: $\delta = 8.04$ and 7.58 (AA′XX′, 4H each; ArH of benzoate rings), 7.39 (s, 4H; ArH), 7.37 (s, 2H; ArH), 7.35 (s, 2H; ArH), 3.94 (s, 6H; OCH_3), 2.86–2.71 (m, 16H; ArCH_2), 1.77–1.62 (m, 16H; ArCH_2CH_2), 1.48–1.26 (m, 48H; CH_2), 0.93–0.82 (m, 24H; CH_2CH_3); ^{13}C NMR: $\delta = 166.4$, 143.6, 142.5, 142.0, 141.9, 133.2, 132.5, 132.4, 131.3, 129.5, 129.4, 128.1, 123.6, 123.2, 122.0, 121.2, 93.6, 93.2, 93.1, 91.5, 81.8, 78.4, 52.1, 34.1, 34.0, 31.8, 31.7, 31.6, 30.6, 30.5, 29.2, 29.1, 22.6, 14.1; elemental analysis calcd (%) for $C_{100}H_{126}O_4$ (1392.09): C 86.28, H 9.12; found: C 86.40, H 9.26; UV/Vis: λ_{max} (ε) = 383 nm (140.19×10^6 cm^{2}mol^{-1}).

General procedure for the preparation of the diacids: KOH in methanol (5N) was added to a solution of the diesters **5** and **7** in THF. The reaction mixture was stirred until no ester was detectable by TLC (hexane/ethyl acetate, 1:1). The THF was then evaporated, and the residue was suspended in a mixture of THF (50 mL) and methanol (50 mL). Trifluoroacetic acid was added until pH 2 was reached. The solvent was then evaporated and the solid residue was washed with cold water until the washings stayed neutral. Finally, the solid was washed with cold (ice bath) THF and with cold hexane. After drying (P_4O_{10}; vacuum) the diacids were ready for further use.

Diacid 6a(H): Reaction of **5a** (0.50 g, 0.59 mmol) in THF (50 mL) with 5N KOH in methanol (35 mL) for 2 d gave **6a(H)** (453 mg, 93%) as a yellow solid. $R_f = 0.28$ (ethyl acetate); m.p. 292 °C (decomp); ^{1}H NMR ($CDCl_3$ + [D$_6$]DMSO, calibration with respect to TMS): $\delta = 8.02$ and 7.57 (AA′XX′, 4H each; ArH of benzoate rings), 7.39 (s, 4H; ArH), 2.86–2.71 (m, 8H; ArCH_2), 1.75–1.59 (m, 8H; ArCH_2CH_2), 1.45–1.27 (m, 24H; CH_2), 0.94–0.82 (m, 12H; CH_3); ^{13}C NMR (THF + $CDCl_3$, calibration with respect to THF): $\delta = 166.1$, 143.8, 142.7, 133.4, 132.6, 131.2, 130.8, 129.8, 127.5, 123.3, 121.6, 94.1, 90.5, 81.6, 78.3, 34.0, 33.9, 31.9, 31.8, 30.8, 30.7, 29.3, 29.2, 22.7, 13.7, 13.6; HRMS: calcd for $C_{58}H_{66}O_4$: 826.496; found: 826.496; UV/Vis: λ_{max} (ε) = 363 nm (81.64×10^6 cm^{2}mol^{-1}).

Diacid 6b(H): Reaction of **5b** (300 mg, 0.22 mmol) in THF (45 mL) with 5N KOH in methanol (10 mL) for 2 d gave **6b(H)** (210 mg, 71%) as a green-yellow solid. $R_f = 0.29$ (ethyl acetate); m.p. 264 °C (decomp); ^{1}H NMR ($CDCl_3$ + [D$_6$]DMSO, calibration with respect to TMS): $\delta =$ 8.04 and 7.58 (AA′XX′, 4H each; ArH of benzoate rings), 7.393 (s, 2H; ArH), 7.387 (s, 2H; ArH), 7.37 (s, 2H; ArH), 7.36 (s, 2H; ArH), 2.88–2.73 (m, 16H; ArCH_2), 1.77–1.60 (m, 16H; ArCH_2), 1.47–1.26 (m, 48H; CH_2), 0.94–0.81 (m, 24H; CH_3); ^{13}C NMR (THF + $CDCl_3$, calibrated with respect to THF): $\delta = 166.3$, 143.5, 142.3, 141.9, 133.2, 132.4, 131.0, 130.4, 129.6, 127.5, 123.7, 123.0, 122.3, 121.1, 93.6, 93.3, 92.9, 90.7, 81.5, 78.3, 34.0, 33.8, 31.8, 31.7, 31.6, 30.7, 30.5, 29.2, 29.0, 22.5, 13.7; FD-MS: *m*/*z* (%): 1365 (100) $[M]^+$, 909.7 (7), 682.0 (43) $[M]^{2+}$; HRMS: calcd for $C_{96}H_{122}$ [$M - 2CO_2$]$^+$: 1274.9547; found: 1274.9543; UV/Vis: λ_{max} (ε) = 384 nm (123.08×10^6 cm^{2}mol^{-1}).

Diacid 8a(H): Overnight reaction of **7a** (0.50 g, 0.89 mmol) in THF (75 mL) with 5N KOH in methanol (35 mL) gave **8a(H)** (0.44 g, 91%) as a colorless solid. $R_f = 0.34$ (ethyl acetate); m.p. 312 °C (decomp); ^{1}H NMR ($CDCl_3$ + [D$_6$]DMSO, calibration with respect to TMS): $\delta = 8.01$ and 7.58 (AA′XX′, 4H each; ArH of benzoate rings), 7.40 (s, 2H; ArH), 2.84–2.76 (m, 4H; ArCH_2), 1.69–1.63 (m, 4H; ArCH_2CH_2), 1.36–1.29 (m, 12H; CH_2), 0.91–0.83 (m, 6H; CH_3); ^{13}C NMR ($CDCl_3$ + [D$_6$]DMSO, calibration with respect to TMS): $\delta = 167.1$, 142.3, 132.3, 131.1, 130.6, 129.5, 127.1, 122.2, 93.4, 90.6, 33.7, 31.3, 30.4, 28.8, 22.2, 14.0; HRMS: calcd for $C_{36}H_{38}O_4$: 534.27701; found: 534.27708; UV/Vis: λ_{max} (ε) = 345 nm (58.10×10^6 cm^{2}mol^{-1}).

Diacid 8b(H): Reaction of **7b** (0.65 g, 0.78 mmol) in THF (90 mL) with 5N KOH in methanol (30 mL) for 1 d gave **8b(H)** (0.55 g, 88%) as a yellow solid. $R_f = 0.41$ (ethyl acetate); m.p. 289 °C (decomp); ^{1}H NMR ($CDCl_3$ + [D$_6$]DMSO, calibration with respect to TMS): $\delta = 8.01$ and 7.58 (AA′XX″, 4H each; ArH of benzoate rings), 7.40 (s, 2H; ArH), 7.37 (s, 2H; ArH), 2.87–2.75 (m, 8H; ArCH_2CH_2), 1.71–1.62 (m, 8H; ArCH_2CH_2), 1.37–1.28 (m, 24H; CH_2), 0.90–0.81 (m, 12H; CH_3); ^{13}C NMR (THF + $CDCl_3$, calibration with respect to THF): $\delta = 166.2$, 142.4, 142.0, 132.5, 131.1, 130.5, 129.7, 127.6, 123.3, 122.3, 93.4, 93.1, 90.8, 34.1, 31.9, 31.8, 30.8, 29.3, 26.4, 24.5, 23.7, 22.6, 13.7; HRMS: calcd for $C_{56}H_{66}O_4$: 802.49611; found: 802.49698; UV/Vis: λ_{max} (ε) = 358 nm (73.35×10^6 cm^{2}mol^{-1}).

Diacid 8c(H): Reaction of **7c** (300 mg, 0.27 mmol) in THF (45 mL) with 5N KOH in methanol (15 mL) for 2 d gave **8c(H)** (245 mg, 84%) as a green-yellow solid. $R_f = 0.45$ (ethyl acetate); m.p. 293 °C (decomp); ^{1}H NMR ($CDCl_3$ + [D$_6$]DMSO, calibration with respect to TMS): $\delta = 8.03$ and 7.58 (AA′XX′, 4H each; ArH of benzoate rings), 7.40 (s, 2H; ArH), 7.38 (s, 4H; ArH), 2.88–2.75 (m, 12H; ArCH_2CH_2), 1.71–1.60 (m, 12H; ArCH_2CH_2), 1.38–1.26 (m, 36H; CH_2), 0.90–0.79 (m, 18H; CH_3); ^{13}C NMR (THF + $CDCl_3$, calibration with respect to THF): $\delta = 165.7$, 142.1, 141.6, 132.1, 130.8, 130.3, 129.4, 127.3, 123.0, 122.6, 121.9, 93.1, 92.8, 92.6, 90.4, 33.8, 31.6, 30.5, 29.0, 22.4, 13.3; HRMS: calcd for $C_{76}H_{94}O_4$: 1070.7152; found 1070.7159; UV/Vis: λ_{max} (ε) = 372 nm (88.76×10^6 cm^{2}mol^{-1}).

General procedure for the formation of the potassium salts 6a,b(K) and 8a–c(K): KOH in methanol (5N, 35–70 mL) was added to a solution of the diester **5** or **7** (0.75–1.00 g) in THF (100 mL). The reaction mixture was stirred until the ester was no longer detectable by TLC (hexane/ethyl acetate, 1:1). The solvent was then evaporated, and the solid residue was washed with cold water until the filtrate stayed neutral. The solid was then washed with ice-cold acetone and finally with ice-cold hexane. The yields were 82–97%. The salts were dried and stored over P_4O_{10} or silica gel. The formation of the potassium salts **6a**,**b(K)**, and **8a–c(K)** was verified by IR spectroscopy.

0947-6539/02/0806-1422 $ 17.50+.50/0 *Chem. Eur. J.* **2002**, *8*, No. 6

General procedure for the preparation of the Cd salts 6(Cd) and 8(Cd), and Pb salts 6(Pb) and 8(Pb): a) $CdCl_2$ or $Pb(NO_3)_2$ in water (0.05 M, 1.1 equivalents) was added to a solution of the respective potassium salt **6(K)** or **8(K)** (50–200 mg) in THF/water (3:1; 40–200 mL) at 40 °C. The precipitated solid was collected by filtration, washed sequentially with water, THF/water (3:1), THF, and acetone, and dried (vacuum, P_4O_{10}). The cadmium and lead salts were stored under argon at −30 °C. The formation of the cadmium and lead salts was monitored by IR spectroscopy[19] and XPS.

b)$CdCl_2$ or $Pb(NO_3)_2$ in water (0.05 M, 1.1 equivalents) was added to a suspension of the respective potassium salt **6(K)** or **8(K)** (150–200 mg) in ethanol/water (1:1; 40–80 mL) at 40 °C. After stirring overnight, the precipitate was collected by filtration, washed sequentially with water, ethanol/water (2:1), ethanol, and acetone, and dried (vacuum, P_4O_{10}). The cadmium and lead salts were stored under argon at −30 °C. The formation of the cadmium and lead salts was monitored by IR spectroscopy[19] and XPS.

General procedure for the preparation of the composites: The Cd or Pb salt was transferred under argon into a small desiccator filled with argon. The desiccator was twice evacuated and refilled with argon. After evacuating the desiccator once more, it was filled with H_2S at room temperature or at 4 °C (reaction carried out in a cool room). The results proved to be independent of the source of H_2S. Wet H_2S was produced by the reaction of sodium sulfide with sulfuric acid. Dry H_2S was obtained from a cylinder and was additionally dried by passage through concentrated sulfuric acid. The reactions were monitored by IR spectroscopy and XPS. They were usually quantitative within 1 h.

Acknowledgement

We thank E. Shavit for assistance in synthesizing the compounds and Prof. L. Leiserowitz for discussions. V.H. thanks the Minerva Foundation for a fellowship. This work was supported by the Israel Ministry of Science, Culture, and Sport, the Petroleum Research Funds of the American Chemical Society through the G.M.J. Schmidt Minerva Center for Supramolecular Architectures, the Danish Foundation for Natural Sciences (DanSync programme), and the European Community (TMR contract ERBFMGECT950059). We thank HASYLAB, DESY, Hamburg (Germany) for beam time, and the Institute of Chemistry of the Freie Universität Berlin for the high-resolution MS analyses.

[1] A. Henglein, *Chem. Rev.* **1989**, *89*, 1861.
[2] L. M. Steigerwald, L. E. Brus, *Acc. Chem. Res.* **1990**, *23*, 183.
[3] H. Weller, *Angew. Chem.* **1993**, *105*, 43; *Angew. Chem. Int. Ed. Engl.* **1993**, *32*, 41.
[4] L. Motte, F. Billoudet, E. Lacaze, J. Doin, M. P. Pileni, *J. Phys. Chem. B* **1997**, *94*, 3104.
[5] C. B. Murray, C. R. Kagan, M. G. Bawendi, *Science* **1995**, *270*, 1335.
[6] C. A. Mirkin, R. L. Lestinger, R. C. Mucic, J. J. Storhoff, *Nature* **1996**, *382*, 607.
[7] A. P. Alivisatos, K. P. Johnson, X. Peng, T. E. Wilson, C. J. Loweth, M. P. Bruchez Jr., P. G. Schultz, *Nature* **1996**, *382*, 609.
[8] N. Feltin, L. Levy, D. Ingert, M. P. Pileni, *J. Phys. Chem. B* **1999**, *103*, 4.
[9] C. P. Collier, T. Vossemeyer, J. R. Heath, *Annu. Rev. Phys. Chem.* **1998**, *49*, *371*.
[10] A. Samokhvalov, M. Berfeld, M. Lahav, R. Naaman, E. Rabani, *J. Phys. Chem. B* **2000**, *104*, 8631.
[11] L. Konopny, M. Berfeld, R. Popovitz-Biro, I. Weissbuch, L. Leiserowitz, M. Lahav, *Adv. Mater.* **2001**, *13*, 580.
[12] S. Guo, L. Konopny, R. Popovitz-Biro, T. Arad, G. Hodes, L. Leiserowitz, M. Lahav, *Adv. Mater.* **1998**, *10*, 657.
[13] S. Guo, L. Konopny, R. Popovitz-Biro, H. Cohen, H. Porteanu, E. Lifshitz, M. Lahav, *J. Am. Chem. Soc.* **1999**, *121*, 9589.
[14] S. Guo, L. Konopny, R. Popovitz-Biro, H. Cohen, M. Sirota, E. Lifshitz, M. Lahav, *Adv. Mater.* **2000**, *12*, 302.
[15] M. Sirota, E. Minkin, E. Lifshitz, V. Hensel, M. Lahav, *J. Phys. Chem. B* **2001**, *105*, 6792.
[16] H. Kukula, S. Veit, A. Godt, *Eur. J. Org. Chem.* **1999**, 277. Compound **1c** was prepared in analogy to **1a**,**b** from the corresponding trimer described in ref. [16].
[17] H. Kukula, Degree Thesis, Johannes-Gutenberg-Universität, Mainz, **1998**.
[18] A. Godt, C. Franzen, S. Veit, V. Enkelmann, M. Pannier, G. Jeschke, *J. Org. Chem.* **2000**, *65*, 7575.
[19] The IR spectra of the powders of **6(Cd,Pb)** or **8(Cd,Pb)** after treatment with H_2S were identical to those obtained from **6(H)** and **8(H)**, respectively. Characteristic changes upon treatment of the salts with H_2S were the appearance of an absorption at $1/\lambda \sim 1690$ cm^{-1} and the disappearance of the absorption lines at $1/\lambda \sim 1579$ and 1382 cm^{-1}.
[20] I. Weissbuch, S. Guo, S. Cohen, R. Edgar, P. Howes, K. Kjaer, J. Als-Nielsen, M. Lahav, L. Leiserowitz, *Adv. Mater.* **1998**, *10*, 117.
[21] I. Weissbuch, P. Baxter, S. Cohen, H. Cohen, K. Kjaer P. Howes, J. Als-Nielsen, G. S. Hanan, U. S. Schubert, J.-M. Lehn, L. Leiserowitz, M. Lahav, *J. Am. Chem. Soc.* **1998**, *120*, 4850.
[22] T. R. Jensen, K. Kjear in *Studies in Interface Science, Vol. 11* (Eds.: D. Möbius, R. Miller), Elsevier, Amsterdam, **2001**, pp. 205–254.
[23] U. H. F. Bunz, V. Enkelmann, L. Kloppenburg, D. Jones, K. D. Shimizu, J. B. Claridge, H. C. zur Loye, G. Lieser, *Chem. Mater.* **1999**, *11*, 1416.
[24] Cerius^2, molecular modeling software for materials research from Biosym molecular simulations, San Diego, CA (USA) and Cambridge (UK).
[25] J. Majewski, R. Edgar, R. Popovitz-Biro, W. G. Bouwmann, J. Als-Nielsen, K. Kjaer, M. Lahav, L. Leiserowitz, *Angew. Chem.* **1995**, *107*, 707; *Angew. Chem. Int. Ed. Engl.* **1995**, *34*, 649.
[26] E. Friedman, H. Cohen, R. Maoz, J. Sagiv, *Langmuir* **1997**, *13*, 5089.

Received: August 6, 2001 [F3470]